Gerald Hörner, Steffen Lau, Zoltan Kantor,
Hans-Gerd Löhmannsröben

Isotope selective analysis of CO2 with tunable diode laser (TDL) spectroscopy in the NIR

first published in:
The Analyst, 129 (2004), pp. 772-778
ISSN: 0003-2654
DOI:10.1117/10.1039/b404552c

ARTICLE

THE ANALYST
www.rsc.org/analyst

Isotope selective analysis of CO_2 with tunable diode laser (TDL) spectroscopy in the NIR

Gerald Hörner, Steffen Lau, Zoltan Kantor† and Hans-Gerd Löhmannsröben*
Institute of Chemistry, Physical Chemistry, Potsdam University, Karl-Liebknecht Str. 24-25, D-14476 Potsdam-Golm, Germany. E-mail: loeh@chem.uni-potsdam.de

Received 25th March 2004, Accepted 2nd June 2004
First published as an Advance Article on the web 6th July 2004

The performance of a home-built tunable diode laser (TDL) spectrometer, aimed at multi-line detection of carbon dioxide, has been evaluated and optimized. In the regime of the $(30^01)_{III} \leftarrow (000)$ band of $^{12}CO_2$ around 1.6 μm, the dominating isotope species $^{12}CO_2$, $^{13}CO_2$, and $^{12}C^{18}O^{16}O$ were detected simultaneously without interference by water vapor. Detection limits in the range of few ppmv were obtained for each species utilizing wavelength modulation (WM) spectroscopy with balanced detection in a long-path absorption cell set-up. High sensitivity in conjunction with high precision —typically ±1‰ and ±6‰ for 3% and 0.7% of CO_2, respectively— renders this experimental approach a promising analytical concept for isotope-ratio determination of carbon dioxide in soil and breath gas. For a moderate $^{12}CO_2$ line, the pressure dependence of the line profile was characterized in detail, to account for pressure effects on sensitive measurements.

1 Introduction

The identification and quantification of factors governing stable isotope abundance in natural systems has been of major interest to geochemists for the past decades.[1,2] Recently, the theoretical concepts and analytical tools used and developed in this field found widespread application in the observation of atmospheric phenomena, biological and biogeochemical processes. The isotope ratios of carbon, nitrogen, oxygen, hydrogen, and sulfur offer an excellent means to obtain basic information about biological process dynamics. Particularly, the isotope ratio of carbon dioxide plays a fundamental role, since CO_2, representing a link between biotic and abiotic domains, can be used as molecular probe in a variety of processes, such as soil organic carbon turn-over.[3–6] Isotope ratios usually are expressed in terms of the so-called δ ("del") notation in per mille (parts per thousand, ‰) relative to a standard material (eqn. (1)). Concerning the stable carbon isotope ratio, material from the Pee Dee Belemnite (PDB) formation in South Carolina serves as a standard.

$$\delta^{13}C = \left(\frac{(^{13}C/^{12}C)_{sample}}{(^{13}C/^{12}C)_{PDB}} - 1 \right) 1000 \qquad (1)$$

Typical $\delta^{13}C$ ratios of natural materials cover the range of *ca.* −50‰ to +10‰. Positive values relative to PDB are restricted to marine carbonate materials. Organic soil components and plant materials usually are strongly depleted in the heavier isotope. Fractionation due to transport or biochemical transformation is commonly limited to a $\delta^{13}C$ variation ($\Delta\delta^{13}C$) of few per mille. Several excellent reviews summarize the origin and extent of isotope effects in atmospheric chemistry as well as in plant ecology and soil science.[7–10]

Though experimentally demanding, isotope-ratio mass spectrometry (IRMS) dominates the field of isotope selective gas analysis. A very high precision of ±0.1‰ is maintained on a routine level, allowing for observation and discussion of small effects.[11] Due to rapid recent developments, sophisticated optical techniques provide more flexible alternatives. A number of studies have addressed important applications for infrared (IR) lasers. Reports include, *e.g.*, isotope selective measurements of water and carbon gases (CO_2 and CH_4) in ambient air in the mid-IR, reaching a precision of ±0.2‰ for CO_2, thus competing with standard IRMS.[12,13] Similar results were obtained by Esler *et al.* using high-resolution FTIR spectroscopy and sophisticated calibration routines for $^{12}C/^{13}C$ isotope ratio determination in atmospheric CO_2 in the field.[14] The same equipment could be also used for trace gas analysis (CH_4, CO, N_2O), thus underlining the flexibility of the method.[15] Non-dispersive IR and laser optogalvanic spectroscopic evaluation of isotope ratios in human breath gas has found application in clinical research.[16,17] These techniques, however, suffer from cross-sensitivity towards water, and therefore require sample preparation. A precision of ±0.22‰ was obtained for a 5% CO_2/N_2 mixture using cavity ring-down spectroscopy.[18] A first isotope selective *in situ* study of atmosphere-ecosystem exchange of carbon dioxide has been conducted by Bowling *et al.*[19] This study comprises sophisticated optical techniques and elaborated biogeochemical concepts.

Near infrared (NIR) diode laser spectrometers are commonly applied in *in situ* measurements of CO_2 and CO in combustion flows.[20,21] Only few groups met the demands of isotope selective measurements of CO_2 on the $\delta^{13}C$ scale also in the NIR. Recently, Chaux and Lavorel obtained a precision of ±5‰ at 1.6 μm in pure CO_2 under reduced pressure.[22] Much better precision (±0.3‰) has been obtained from analysis of the stronger lines at 2.0 μm with a concentration of 2% CO_2 in N_2.[23,24] Werle has provided a recent review of spectroscopic applications of NIR lasers.[25]

In this paper we demonstrate the performance of a tunable diode laser (TDL) spectrometer, working around 1.6 μm, concerning simultaneous multi-line detection of carbon dioxide (for a spectral overview see Fig. 1). In particular, the opportunities and limitations with respect to high-precision isotope ratio evaluation in this wavelength regime are discussed. The TDL spectrometer has been evaluated for isotope-ratio determination of carbon dioxide in ambient air (typically 350 ppmv CO_2), in soil gas (typically 1,000–20,000 ppmv CO_2), and in breath gas (typically 30,000–50,000 ppmv CO_2). The stability and precision of the experimental set-up is examined by replicate measurements and evaluation of the limits of detection (LOD). For a moderate $^{12}CO_2$ line, the pressure dependence of the line profile is characterized in detail, to account for pressure effects on isotope selective measurements.

2 Experimental

Fig. 2 depicts the experimental set-up for isotope selective TDL spectroscopy. The spectrometer is based on a temperature stabilized external-cavity-diode-laser (ECDL; TEC 500 Sacher La-

† Present address: Department of Physics, University of Veszprem, Egyetem u. 10, H-8200 Veszprem, Hungary.

DOI: 10.1039/b404552c

sertechnik, Marburg, Germany) with a maximum output power of 8 mW and an emission line width of $< 1 \times 10^{-4}$ cm^{-1}. The laser is tunable within the spectral range of 6,000 to 6,400 cm^{-1} *via* mechanical manipulation of the cavity. Fine tuning is achieved by piezoelectrically controlled setting of the cavity. The mode hopping-free spectral range is 1.0 cm^{-1}. The laser light is divided into a sampling and a reference beam by a 50% beam splitter. After passage of a second 50% beam splitter in the reference path, 25% of the total emitted power is detected with a room-temperature InGaAs photodiode (reference detector PD-2). A wavemeter (WM)

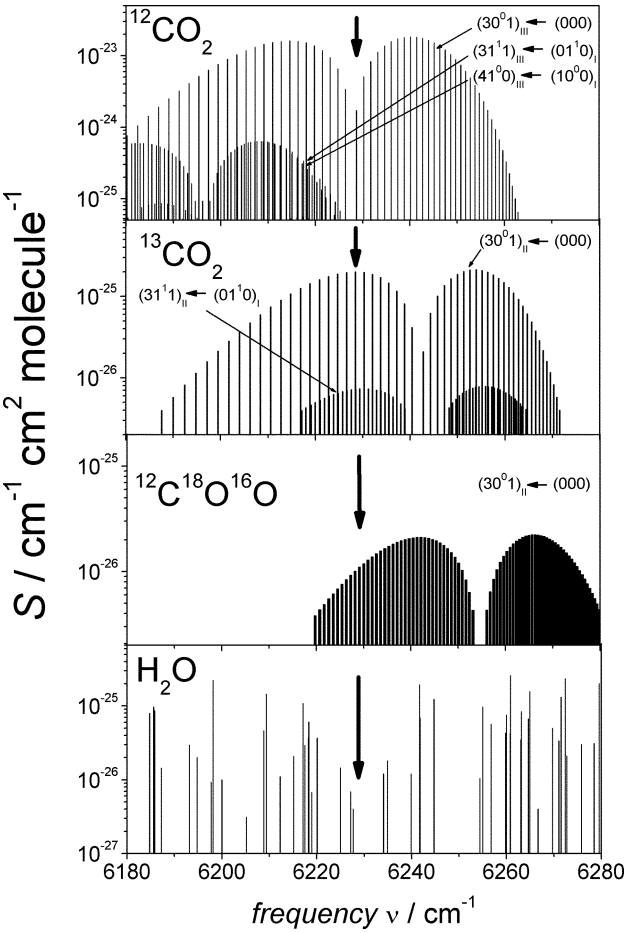

Fig. 1 Tabulated line strengths S of the main isotope species of CO_2 and of water in the ro-vibrational bands around 1.6 μm (from the HITRAN database, $^{12}CO_2$ main band: $(30^01)_{III} \leftarrow (000)$, S values given for 296 K include isotope natural abundances with relative percentages $^{12}C^{16}O_2$: 98.420; $^{13}C^{16}O_2$: 1.106; $^{12}C^{18}O^{16}O$: 0.395; arrows indicate the studied spectral range in which no strong water lines are found).[26]

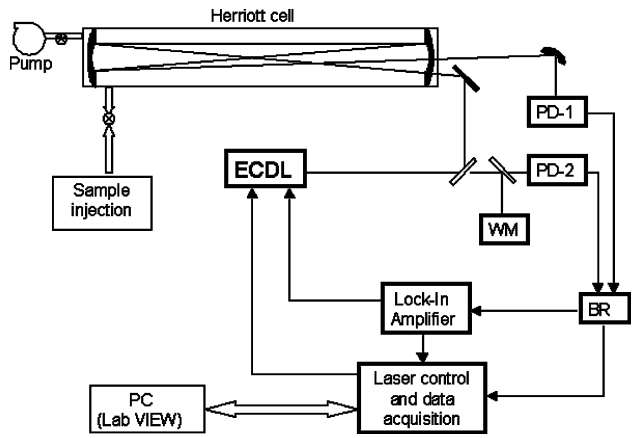

Fig. 2 Scheme of the TDL spectrometer; optical path simplified for clarity (see text for abbreviations).

(Burleigh WA-1100, Harpenden, UK) is used for wavelength and output power control. To avoid parasitic feedback from the WM mirrors to the laser, this beam is blocked during measurement. A planar mirror in the sampling path directs the laser light into a Herriott-type multi-pass-cell (MPC1000S; Scienca Industria Tecnologia, Florence, Italy; tube length 1.12 m; volume 8.25 l), equipped with two confocal gold mirrors (reflectivity at 1.6 μm > 98.2%) yielding a total light path of 100.9 m. The outcoming beam is focussed on another InGaAs photodiode (sample detector PD-1) by an aspheric mirror. The photocurrents of the detectors are processed by a balanced receiver (BR V 1.0, Adrop, Nuremberg, Germany).

Frequency tuning and modulation is performed by a piezoelectric system. The laser emission (frequency ν_L) is periodically scanned over a spectral range of *ca.* 0.5 cm^{-1} by applying a triangular-shaped voltage to the piezo crystal with a scan frequency f_s of 0.033 Hz. Higher repetition rates induce growing wavelength hysteresis of the laser output. Rise and fall time of the piezo-voltage are set to 15 and 5 s, respectively. Individual scans are separated by a time delay of 10 s for the sake of laser relaxation. The complete frequency scanning program is PC-controlled (Lab VIEW).

For noise reduction a wavelength modulation (WM) technique is employed.[27–29] The piezo-voltage, which controls ν_L, is superimposed by a small oscillating voltage (modulation frequency f = 800 Hz, typical modulation amplitude $\delta\nu$ = 0.02 cm^{-1}) from the modulation output channel of a digital lock-in amplifier (EG&G 7260 DSP Lock-In, Wokingham, UK). The AC-coupled output of the BR is processed by the lock-in amplifier (harmonic detection; low-pass filtering). The time constant is 100 ms with 12-dB/oct digital filtering, giving a detection bandwidth of 2.5 Hz. Output signals are transferred to a 16-bit data-acquisition-system (DAS D1614, Department of Experimental Physics, University of Szeged, Hungary) and subsequently sent to a PC for further processing. One spectrum consists of 2048 points.

Ideally, WM spectroscopy is a zero-baseline technique. Due to the small emission bandwidth of the probing laser and imperfect antireflection surfaces, optical interference fringes usually form sinusoidal background signals, superimposed with the spectra of interest. Since the dominant fringes are relatively stable for several minutes, subtractive background correction with the response from the evacuated cell (residual pressure $< 10^{-5}$ bar) is performed. Overall, a measurement cycle, including evacuation, background measurement, sample gas purging, and sample measurement is conducted within 4 min. 300 to 50,000 ppmv CO_2/N_2 gas mixtures (from Messer-Griesheim, Darmstadt, Germany) were used as concentration standards without further preparation. CO_2 concentrations below 300 ppmv were obtained by dilution of a 300 ppmv reference sample with CO_2-free synthetic air. Breath gas samples were introduced into the absorption cell without preparation. The samples were injected into the MPC by hypodermic needles through a Teflon septum, to be exchanged after each 20 injections. The leakage rate was approximately 0.1 to 0.5 mbar per day, thus the leak error throughout the total background and sample measurement period was negligible.

3 Theory and spectral analysis

Since fundamentals of WM spectroscopy with tunable diode lasers have been described in detail elsewhere,[27–29] only a brief summary is given here. Light attenuation in absorbing media is quantified by Beer's law (eqn. (2)), with the light intensities $I_0(\nu)$ (non-attenuated) and $I(\nu)$ at frequency ν (in cm^{-1}), the number density of absorber N (in molecules cm^{-3}), the optical path length L (in cm), and the absorption cross-section $\sigma(\nu)$ (in cm^2 per molecule). The latter comprises the line strength S (in cm^{-1} cm^2 per molecule) and the pressure-dependent absorption profile shape function $g(\nu)$ (in cm), also called line shape function.

$$I(\nu = I_0(\nu) \exp(-\sigma(\nu) NL) \quad (2)$$

The attenuation at the center of an absorption line is both dependent on absorber number concentration and total pressure. The influence of temperature on line strengths results from Boltzmann distribution of population densities.[27] The absorption lines highlighted in Table 1 exhibit a small but distinct temperature dependence (*e.g.* for a temperature increase of 1 K, −3.4 and −1.6‰ for $^{12}CO_2$ *R*(0) and $^{13}CO_2$ *P*(16), respectively). However, larger temperature effects (up to almost +30‰) are obtained for the $^{12}CO_2$ (*R*(38), *R*(57)) and the $^{13}CO_2$ (*P*(18)) satellite lines, suspected to overlap at least in part with the wings of the major lines. As a consequence, rather than considering total peak areas, quantitative analysis in the following is based on evaluation of signal intensities at the line centers. Using tabulated values for *S* and the air broadening coefficient γ_{air} (see Table 1), for known pressure and absorber concentrations, line widths $\Delta\nu$ (in cm^{-1}, referring to full widths at half maximum, FWHM) and absorbances are calculated. For a total pressure p = 150 mbar at atmospheric CO_2 concentration (350 ppmv) absorption coefficients at the line center ($\alpha_{max} = \sigma_{max}N$) cover the range of 10^{-10} to 10^{-7} cm^{-1}. Taking into account the path length (L = 100.9 m), absorbances of as low as 10^{-6} to 10^{-3} are expected under our experimental conditions.

Conventional absorption spectroscopy therefore has to deal with the problem that very small transmission alterations usually are superimposed by huge background signals. Contrarily, WM techniques provide a powerful means for background reduction, since they discriminate signals strongly by curvature. Narrower signals are enhanced, while broader features suffer considerable attenuation. While the laser frequency ν_L is scanned linearly across an absorption line, a high frequency sinusoidal voltage modulates the laser output around the instantaneous emission frequency with a modulation amplitude $\delta\nu$ and a modulation frequency f (in Hz), *cf.* eqn. (3):

$$\nu = \nu_L + \delta\nu\cos(ft) \quad (3)$$

The transmitted light intensity can be expressed as a Fourier series. The Fourier components $A_{nf}(\nu_L)$ at the harmonics of f are each proportional to the absorber concentration.[29] Individual components $A_{nf}(\nu_L)$ are measured by a lock-in amplifier. Only for small modulation amplitudes, direct proportionality between the *n*th derivative of the absorption line profile $\sigma(\nu)$ and the Fourier component of the *n*th harmonic is obtained. Usage of modulation amplitudes close to the line width induces a substantial increase of signal strength and sensitivity, but also a deviation from proportionality. In the following, the values measured by the lock-in amplifier are denoted as *nf*-amplitudes (A_{nf}) and are given in volts.

Fig. 3 shows harmonic spectra ($1 \le n \le 5$) obtained for a 6,900 ppmv mixture of CO_2 in N_2 at 60 mbar. The main absorption lines $^{12}CO_2$ *R*(0) and $^{13}CO_2$ *P*(16) are resolved at this pressure. A small feature at 6,228.61 cm^{-1}, partially overlapping with the *R*(0), is identified as the $^{12}CO_2$ *R*(57) line (see inset). The $^{12}CO_2$ *R*(38) and the $^{13}CO_2$ *P*(18) lines cannot be resolved from the dominating main lines. Noise levels are calculated from the spectra as the root-mean-square of base-line deviation in absorption free spectral regions. Individual signal-to-noise-ratios (SNR) are calculated for each harmonic. The SNR is maximized for the 2nd harmonic detection. Though noise suppression is even more pronounced for the higher harmonics, this effect is predominated by the substantial signal loss. From the SNR data for the 2nd harmonic spectra, the least detectable absorbance is estimated to 2×10^{-6}. This value, based on a SNR of 1 at 1 Hz noise-bandwidth, is in good agreement with the results of other groups with similar experimental setups.[30–32] By use of sophisticated high-frequency modulation spectroscopy, detectable absorbance levels of 10^{-8}, in the range of shot-noise, are reported.[33,34] This significantly higher sensitivity is achieved only

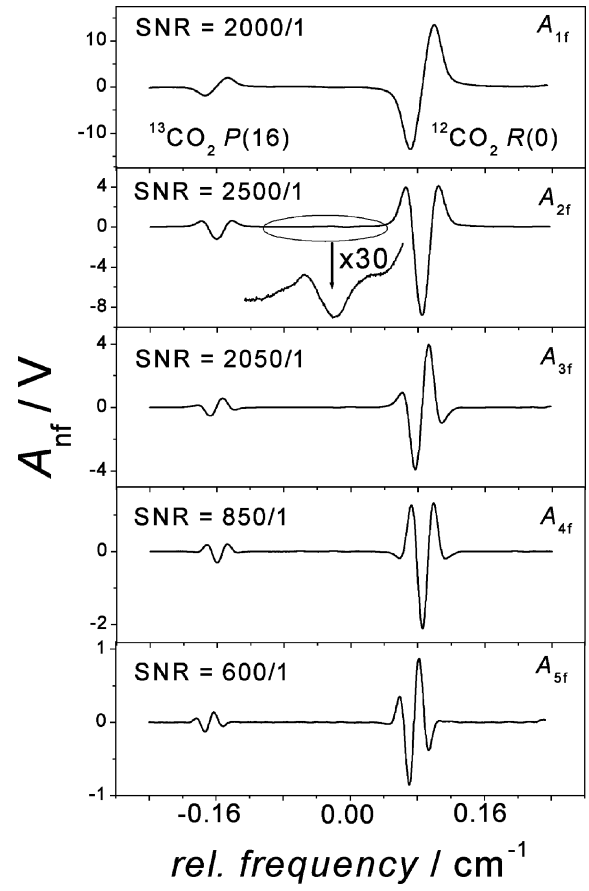

Fig. 3 Harmonic amplitude A_{nf} detection of the $^{12}CO_2$ *R*(0) and the $^{13}CO_2$ *P*(16) lines of CO_2 in N_2 (6900 ppmv) at a total pressure of 60 mbar; inset highlights the $^{12}CO_2$ *R*(57) line, scaled-up by a factor of 30 (single-scan spectra, background corrected; frequency scale centered at 6,228.55 cm^{-1}; modulation frequency f_m = 800 Hz; lock-in time-constant 100 ms with detection bandwidth of 2.5 Hz, modulation voltage U_{osc} 25 mV corresponding to modulation amplitude $\delta\nu$ = 0.0275 cm^{-1}; settings optimized for 2nd harmonic detection; SNR based on the $^{12}CO_2$ *R*(0) line; note different ordinate scales).

Table 1 Overview of spectral data for CO_2 absorption lines in the spectral window around 6,228.5 cm^{-1} (HITRAN data base);[26] major lines under investigation are given, minor adjacent lines are in italic; the $^{12}CO_2$ *P*(16) line was used for detection limit determination

Species	Frequency ν/cm^{-1}	S^a/ cm^{-1} cm^2 $molec^{-1}$	E''^b/cm^{-1}	$(S_T - S)/S^a$ (‰)	γ_{air}^c/ cm^{-1} bar^{-1}	Line
$^{12}CO_2$	6,228.163	2.64×10^{-26}	1664.2	+24.2	0.1299	*R*(50)
$^{12}C^{18}O^{16}O$	6,228.202	1.01×10^{-26}	388.7	+3.0	0.1346	*P*(32)
$^{13}CO_2$	6,228.436	2.00×10^{-25}	106.1	−1.6	0.1461	*P*(16)
$^{13}CO_2$	*6,228.484*	*7.42×10^{-27}*	*782.3*	*+9.5*	*0.1437*	*P*(18)
$^{12}CO_2$	*6,228.611*	*7.42×10^{-27}*	*1957.4*	*+29.1*	*0.1269*	*R*(57)
$^{12}CO_2$	6,228.690	1.71×10^{-24}	0	−3.4	0.1874	*R*(0)
$^{12}CO_2$	*6,228.726*	*1.32×10^{-26}*	*1966.2*	*+29.2*	*0.1331*	*R*(38)
$^{12}CO_2$	*6,214.588*	1.65×10^{-23}	106.1	−1.6	0.1461	*P*(16)

[a] *S* is given for 296 K, the relative temperature variation in line strengths is calculated with S_T for 297 K.[27] [b] Lower state energy of the transition. [c] Air-broadening (FWHM) coefficients.

with far more expensive and experimentally demanding equipment.

4 Characterization of the TDL spectrometer

a Pressure dependence and experimental broadening coefficients

Conditions for optimized sensitivity have to compromise between highest signal strength possible and minimal pressure broadening of the signal. Direct absorption measurements usually yield proportionality between signal strength and pressure only for small values of p. Due to collision broadening of the line profile, the absorbance at line centre approaches a constant value with increasing pressure. However, proportionality is retained between peak area and p. In the case of 2nd harmonic detection, the observed 2f-line shape is strongly influenced by detection system parameters, particularly the modulation amplitude, $\delta\nu$. Signal intensity is maximized if modulation amplitude and absorption line width are almost equal ($\delta\nu \approx 1.1\Delta\nu$). Higher modulation causes signal broadening, damping (illustrated by the $^{12}CO_2$ $R(0)$ line in Fig. 4a), and, in extreme, line symmetry losses. This signal broadening convolutes to the real line profile function. In the low-pressure regime ($p < 80$ mbar) proportionality of signal amplitude and pressure is fulfilled. Both the line centre 2f-amplitude (Fig. 4b) and the peak area exhibit decreasing values in the high-pressure domain. Approaching ambient pressure, the absorption bands were not resolved, due to strong overlap. As a main consequence of the spectrometer characteristics, the mentioned interplay of signal strength and line width defines an optimal pressure range of $50 < p < 150$ mbar. For our cell, the corresponding sample volumes are of $400 < V_s < 1{,}200$ cm^3. The choice of pressure conditions therefore not only reflects the analytical problem, but has to consider sample accessibility and abundance as well. Considering analysis of natural systems, we have chosen 60 mbar (V_s = 500 cm^3) as default pressure.

In the 50–150 mbar pressure regime the resulting line shape at ambient temperature is made up by Doppler and collision broadening (Voigt profile). In contrast to direct absorption spectroscopy, the extraction of exact line width values from harmonic spectra in the Voigt regime is not straightforward. From either purely Doppler- (*ca*. $p < 10$ mbar) or collision-broadened ($p > 150$ mbar) 2f-spectra, experimental line widths can be obtained directly: in the collision broadening regime, the FWHM of the underlying Lorentzian transforms to the frequency difference of the secondary 2f-maxima in the harmonic spectra. In the case of Doppler-broadened lines, the FWHM of the Gaussian is approximated in the 2f-notation as the frequency distance of the zero-crossings scaled by the factor of $(2\ln 2)^{\frac{1}{2}}$.

Voigt profile line widths $\Delta\nu_{Voigt}$ can approximately be calculated by eqn. (4).[27] The Doppler ($\Delta\nu_{Doppler}$) and collision ($\Delta\nu_p$) line widths are obtained from well known gas kinetic (eqn. (5), with T in K and M in g mol^{-1}) and empiric (eqn. (6)) relations:[27,28]

$$\Delta\nu_{Voigt} = 0.5346\Delta\nu_p + \sqrt{0.2166\Delta\nu_p^{\,2} + \Delta\nu^2_{Doppler}} \quad (4)$$

$$\Delta\nu_{Doppler} = 7.162\cdot 10^{-7}\nu_0\sqrt{T/M} \quad (5)$$

$$\Delta\nu_P = \gamma_{air} p (T_0/T)^n \quad (6)$$

For 292 K and ν_0 = 6,228.690 cm^{-1} for the line center frequency, a Doppler width of 0.0115 cm^{-1} is obtained for the $^{12}CO_2$ $R(0)$ line. For evaluation of $\Delta\nu_p$, the tabulated value of the air broadening coefficient γ_{air} (0.1874 cm^{-1} bar^{-1}, see Table 1) comes to use. The temperature dependence of the pressure broadening contains the empirical coefficient n = 0.74.[26] Shown in Fig. 5 are the experimentally determined and the calculated line widths $\Delta\nu$ for a pressure range covering three orders of magnitude. Despite the simplified approaches, the experimental and calculated line widths are in excellent agreement in the regime of collision broadening. A slight but systematic overestimation of $\Delta\nu$ is evident for the Doppler-broadened lines. This is supposed to result from the fact that the 2nd derivative and the 2nd harmonic signals are not strictly proportional.

In order to evaluate the performance of the TDL spectrometer, pressure broadening of the $^{12}CO_2$ $R(0)$ line was investigated in four gases in the pressure range 150–1000 mbar. CO_2 concentrations were 6,900 ppmv for the experiments in nitrogen and air, and 10,400 ppmv for the experiments in argon. Under these conditions the contributions of self-broadening can be neglected. Line profiles are attributed to be purely collision broadened, *i.e*. of Lorentzian line shape. The line widths $\Delta\nu$ obtained in dependence of the total pressure are shown in the inset of Fig. 5. Slopes of the linear fits directly provide the broadening coefficient γ. The good (self-broadening) or very good (air-broadening) agreement of experimental and literature data underlines the reliability of the spectrometer set-up and data processing routines (see Table 2).

b Sensitivity: The limits-of-detection (LOD) and multi-species analysis

In order to evaluate the sensitivity of the TDL spectrometer, 2nd harmonic spectra of the strong absorption line at 6,214.59 cm^{-1}

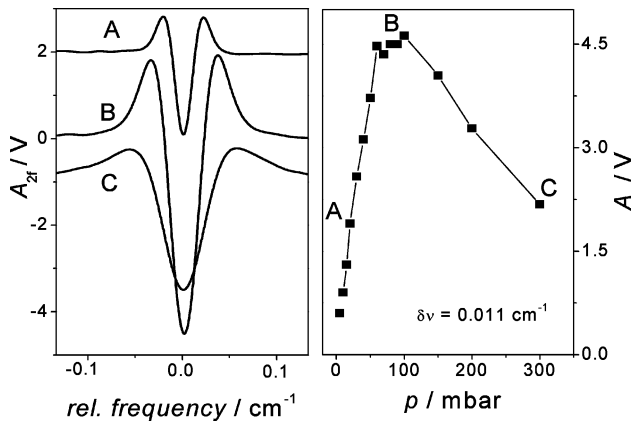

Fig. 4 2nd harmonic detection of the $^{12}CO_2$ $R(0)$ line for 6900 ppmv CO_2 in N_2 (Lock-in time constant 100 ms, modulation frequency 800 Hz, modulation amplitude 0.011 cm^{-1}); (a) absorption spectra for three exemplary pressures (A: 20 mbar, B: 100 mbar, C: 300 mbar), offset for clarity; (b) Pressure dependence of the A_{2f} amplitudes at line center, A, in absolute values.

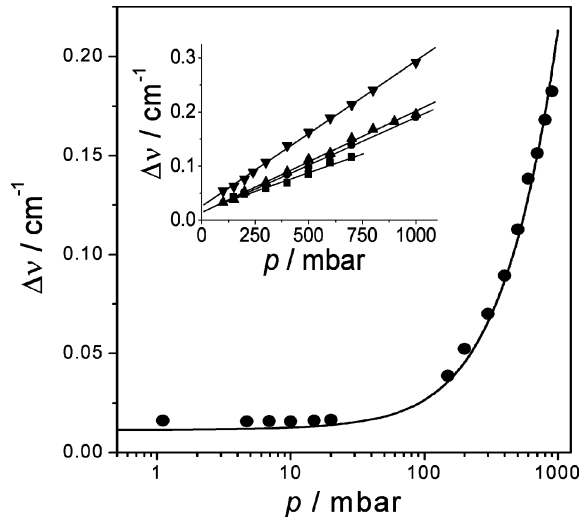

Fig. 5 Line widths $\Delta\nu$ (FWHM) of the $^{12}CO_2$ $R(0)$ line for a concentration of 6900 ppmv in N_2 in dependence of sample pressure (experimental data as points; line calculated from eqn. (4)); Inset: Pressure dependence of experimental line widths $\Delta\nu$ of the $^{12}CO_2$ $R(0)$ line in pure CO_2 (downward triangles), air (upward triangles), N_2 (circles), and Ar (squares) at 292 K (lines are linear fits to the measured data ($R^2 > 0.993$)).

($^{12}CO_2$ *P*(16)) were measured in the concentration range of 30 to 6,900 ppmv. In the low concentration regime, the plot of the line-center amplitudes (derived from spectra in Fig. 6a), against the overall concentration reveals good linearity (Fig. 6b). The LOD for this line was determined as 2 ppmv.

$$\mathrm{LOD} = \frac{2\sigma(A_0)}{m} \qquad (7)$$

The given limits of detection are calculated according to eqn. (7) from the standard deviation of the intercept ($\sigma(A_0)$, in Volts) and the slope (*m*, in Volts per ppmv) of the linear signal-concentration plots (Figs. 6–8).

Due to the broad tuning range of the ECDL, a variety of species can be determined quantitatively and simultaneously. However, simultaneous multi-species detection demands for compromise with respect to the individual sensitivities. Not in every case are the strongest lines of the different species accessible in a single spectral window. Fig. 7a comprises exemplary spectra of a weak $^{12}C^{16}O_2$ and a moderate $^{12}C^{18}O^{16}O$ line. For comparison, also two human breath gas samples were injected and measured. As expected, water does not interfere with the investigated carbon dioxide lines. This is important for breath and soil gas analysis, where water concentrations usually reach saturation. As detection limits, 900 and 7 ppmv are obtained for $^{12}C^{16}O_2$ and $^{12}C^{18}O^{16}O$ from linear plots of the line center amplitudes (Fig. 7b). For the latter molecule, a relative percentage of 0.395 (according to PDB standard) is assumed for calculation. Regarding $^{16}O/^{18}O$ isotope ratio determination, the achieved sensitivity is expected to be sufficient for pure CO_2, whereas the smaller concentrations in human breath (30,000 to 50,000 ppmv) still demand improved baseline stability. Corresponding LOD are derived as 20 and 1 ppmv for a pair of $^{12}CO_2$ and $^{13}CO_2$ lines, also suitable for simultaneous detection, (for exemplary spectra and calibration plots, see Fig. 8). For the ^{13}C line a relative percentage of 1.106 is assumed (PDB standard). The achieved spectrometer stability is expected to be sufficient for precise $^{12}C/^{13}C$ isotope ratio determinations in soil gases. A double logarithmic plot of 2*f*-amplitudes *versus* carbon dioxide concentration (Fig. 9) summarizes the results of the concentration measurements presented above. Linearity is maintained over a large concentration range covering three orders of magnitude. The slopes have the expected value of unity. For example, the $^{12}CO_2$ *R*(0) and $^{13}CO_2$ *P*(16) lines, chosen for isotope ratio determination, show excellent agreement herewith (1.006 ± 0.007 and 1.000 ± 0.014, respectively).

5 Spectroscopic evaluation of $^{12}C/^{13}C$ isotopic ratios of CO_2

Based on SNR considerations (see Fig. 3), an optimal isotope ratio resolution of *ca*. ±3.0‰ is expected for a concentration of 6,900 ppmv. This improves to ±1.0‰ measured for a higher CO_2 concentration of 30,000 ppmv, typical for human breath. The overall experimental precision is evaluated from complete fill–measurement–evacuation–refill cycles. The results of 10 such cycles for a sample concentration of 6,900 ppmv at 60 mbar are shown in Fig. 10.

For the $^{12}CO_2$ line the mean amplitude equals to 10.475 V with a standard deviation of ± 49 mV (±4.8‰). The respective values for the $^{13}CO_2$ are 1.538 V ± 11 mV (±7.1‰). The corresponding $^{12}C/^{13}C$ amplitude ratios result in a mean value of 6.81 ± 0.04 (±6‰).

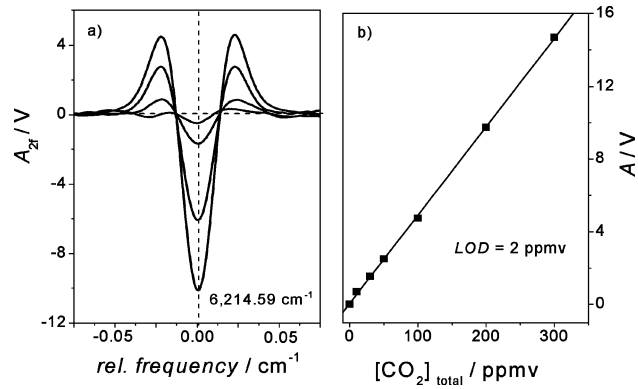

Fig. 6 (a) 2*f*-spectra of the $^{12}CO_2$ *P*(16) line for concentrations of 10 to 200 ppmv of CO_2 in synthetic air (p = 60 mbar); (b) line center amplitudes *A* (absolute values) in dependence of concentration; points: experimental data; line: linear fit (R^2 = 0.9998).

It is notable that the overall isotope precision achieved in replicate measurements here, namely ±6‰ for 6,900 ppmv CO_2/N_2 at 60

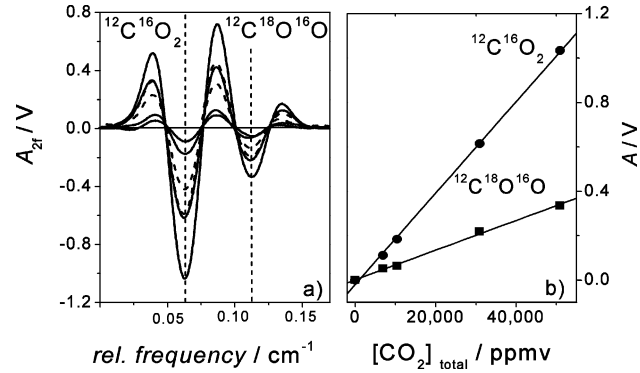

Fig. 7 (a) 2nd harmonic spectra of the $^{12}C^{16}O_2$ *R*(50) and $^{12}C^{18}O^{16}O$ *P*(32) lines of CO_2 in N_2 in the concentration range from 6,900 to 50,900 ppmv; dashed lines correspond to breath gas samples, injected without sample preparation; all spectra obtained at p = 60 mbar; (b) 2*f*-amplitudes in line center *A* (absolute values) *versus* total concentration for $^{12}C^{16}O_2$ and $^{12}C^{18}O^{16}O$; symbols: experimental data; lines: linear fits.

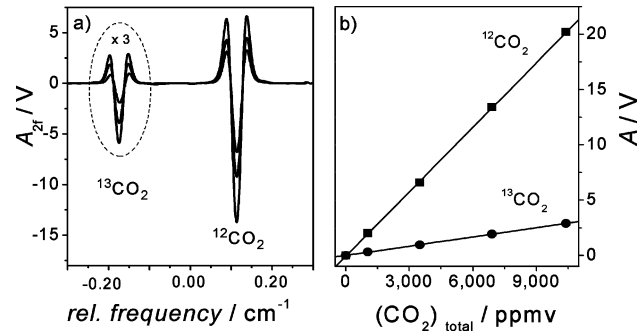

Fig. 8 (a) Exemplary 2nd harmonic spectra of the $^{12}CO_2$ *R*(0) and the $^{13}CO_2$ *P*(16) lines for concentrations in the range of 1000 to 7000 ppmv; pressure p = 60 mbar; wavenumber scale centered at 6,228.55 cm^{-1}; $^{13}CO_2$ lines scaled by a factor of three for comparison; (b) 2*f*-amplitudes (absolute values) for $^{12}CO_2$ and $^{13}CO_2$ in line center *versus* total concentration; symbols: experimental data; lines: linear fits.

Table 2 Experimental broadening coefficients γ at 292 K for the $^{12}CO_2$ *R*(0) line

	γ_{CO2}/cm^{-1} bar^{-1}	γ_{air}/cm^{-1} bar^{-1}	γ_{N2}/cm^{-1} bar^{-1}	γ_{Ar}/cm^{-1} bar^{-1}
Experimental	0.268 (0.003)	0.187 (0.004)	0.177 (0.004)	0.138 (0.007)
Tabulated[a]	0.2526	0.1874	—	—

[a] Tabulated values taken from HITRAN96,[26] numbers in brackets denote the standard deviation of the coefficients.

mbar (path length 109 m), is superior to the precision of ±5‰ for the analysis of 2.5 mbar pure CO_2 (path length 32 m) reported in a recent TDL study at 1.6 μm.[22] From the values in Table 1 a theoretical line center ratio of 6.58 is obtained. Working pressure and ambient temperature have been accounted for in the calculation. It is felt that experimental and calculated ratios are close enough to be satisfying at present. However, quantitative comparison of the given values would demand for calibration with isotopically certified samples. This task marks the oncoming experimental challenge.

6 Conclusions

A highly sensitive and selective TDL spectrometer, working at 1.6 μm, has been developed and implemented. The chosen experimental approach, based on the broad tuning range of an ECDL, offers a great deal of experimental versatility. With the very same set-up, both sensing of numerous trace compounds and quantitative analysis of simultaneously recorded species can be performed. For three isotope species of carbon dioxide, detection limits in the lower ppmv range were obtained. Absorption line parameters (broadening coefficients) derived from harmonic spectra were in good agreement with tabulated values. The overall experimental results regarding pressure effects, detection limits, and precision of 2nd harmonic detection, provide the base for determination of isotope ratios in carbon dioxide with high precision. At present, residual background fluctuations in the harmonic spectra prevent high-precision measurements at atmospheric concentration levels. For the higher concentrations in soil systems or breath gas samples, satisfying or good precision is obtained. Improvements in sensitivity and precision are expected from a further optimization of the spectrometer optics. Particularly the dampening of parasitic optical feedbacks is going to be addressed.

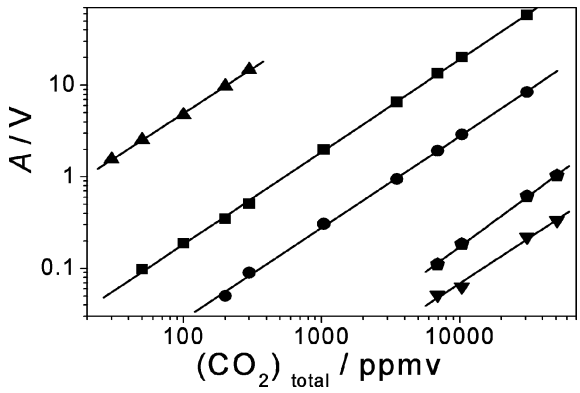

Fig. 9 Double logarithmic plot of 2*f*-line center amplitudes *A* and total carbon dioxide concentration for the five absorption lines under investigation (upward triangles: $^{12}CO_2$ *P*(16); squares: $^{12}CO_2$ *R*(0); circles: $^{13}CO_2$ *P*(16); pentagons: $^{12}CO_2$ *R*(50); downward triangles: $^{12}C^{18}O^{16}O$ *P*(32)); lines: linear fits.

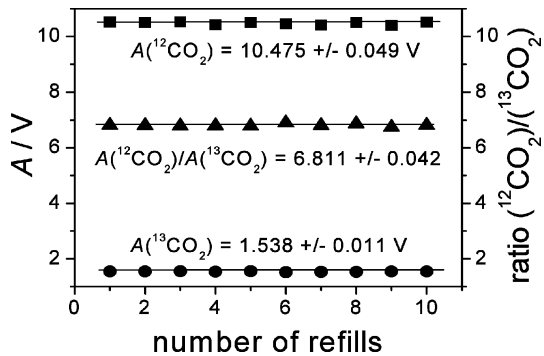

Fig. 10 Line center 2*f*-amplitudes *A* of the $^{12}CO_2$ *R*(0) (squares) and the $^{13}CO_2$ *P*(16) (circles) lines obtained for 6,900 ppmv CO_2/N_2 at 60 mbar; iterative runs performed as fill–evacuation–refill cycles; triangles: Ratio of the ^{12}C and ^{13}C amplitudes.

Acknowledgements

Funding of the project by the Deutsche Forschungsgemeinschaft in the priority program SPP 1090 ("Soils as sources and sinks of CO_2") is gratefully acknowledged. The authors thank Dr Frank Schael (now with Ehrfeld Mikrotechnik AG) for important contributions in the initial phase of the work and Dr R. Engelbrecht (Institut für Hochfrequenztechnik, Universität Erlangen-Nürnberg) for helpful advice regarding optimized electronic detection.

References

1 J. Hoefs, *Stable Isotope Geochemistry*, Springer, Berlin, 5th edn., 2004.
2 W. H. Schlesinger, *Biogeochemistry—An Analysis Of Global Change*, Academic Press, San Diego, 2nd edn., 1997.
3 J. Balesdent, A. Mariotti and B. Guillet, *Soil Biol. Biochem.*, 1987, **19**, 25–30.
4 M. Bernoux, C. C. Cerri, C. Neill and J. F. L. de Moraes, *Geoderma*, 1998, **82**, 43–58.
5 I. Del Galdo, J. Six, A. Peressottis and M. F. Cotrufo, *Global Change Biol.*, 2003, **9**, 1204–1213.
6 B. John, B. Ludwig and H. Flessa, *Soil Biol. Biochem.*, 2003, **35**, 1193–1202.
7 R. Amundson, L. Stern, T. Baisden and Y. Wang, *Geoderma*, 1998, **82**, 83–114.
8 R. Amundson, *Annu. Rev. Earth Planet. Sci.*, 2001, **29**, 535–562.
9 T. E. Dawson, S. Mambelli, A. H. Plamboeck, P. H. Templer and K. P. Tu, *Annu. Rev. Ecol. Syst.*, 2002, **33**, 507–559.
10 C. A. M. Brenninkmeijer, C. Janssen, J. Kaiser, T. Röckmann, T. S. Rhee and S. S. Assonov, *Chem. Rev.*, 2003, **103**, 5125–5161.
11 I. T. Platzner, *Modern Isotope Ratio Mass Spectrometry*, Wiley & Sons, Chichester, 1997.
12 E. R. T. Kerstel, R. van Trigt, N. Dam, J. Reuss and H. A. J. Meijer, *Anal. Chem.*, 1999, **71**, 5297–5303.
13 J. B. McManus, M. S. Zahniser, D. D. Nelson, L. R. Williams and C. E. Kolb, *Spectrochim. Acta A*, 2002, **58**, 2465–2479.
14 M. B. Esler, D. W. T. Griffith, S. R. Wilson and L. P. Steele, *Anal. Chem.*, 2000, **72**, 216–221.
15 M. B. Esler, D. W. T. Griffith, S. R. Wilson and L. P. Steele, *Anal. Chem.*, 2000, **72**, 206–215.
16 M. Haisch, P. Hering, W. Fabinski and M. Zöchbauer, *Tech. Mess.*, 1996, **63**, 322–328.
17 V. Savarino, F. Landi, P. Dulbecco, C. Ricci, L. Tessieri, R. Biagini, L. Gatta, M. Miglioli, G. Celle and D. Vaira, *Dig. Dis. Sci.*, 2000, **45**, 2168–2174.
18 E. R. Crosson, K. N. Ricci, B. R. Richman, F. C. Chilese, T. G. Owano, R. A. Provencal, M. W. Todd, J. Glasser, A. A. Kachanov, B. A. Paldus, T. G. Spence and R. N. Zare, *Anal. Chem.*, 2002, **74**, 2003–2007.
19 D. R. Bowling, S. D. Sargent, B. D. Tanner and J. R. Ehleringer, *Agric. For. Meteorol.*, 2003, **118**, 1–19.
20 R. M. Mihalcea, D. S. Baer and R. K. Hanson, *Appl. Opt.*, 1998, **37**, 8341–8347.
21 E. Webber, S. Kim, S. T. Sanders, D. S. Baer, R. K. Hanson and Y. Ikeda, *Appl. Opt.*, 2001, **40**, 821–828.
22 R. Chaux and B. Lavorel, *Appl. Phys. B*, 2001, **72**, 237–240.
23 P. Werle, R. Mücke, F. D'Amato and T. Lancia, *Appl. Phys. B*, 1998, **67**, 307–315.
24 G. Gagliardi, A. Castrillo, R. Q. Iannone, E. R. T. Kerstel and L. Gianfrani, *Appl. Phys. B*, 2003, **77**, 119–124.
25 P. Werle, in *Laser in Environmental and Life Sciences*, ed. P. Hering, J. P. Lay and S. Stry, Springer, Berlin, 2004, pp. 223–244.
26 L. S. Rothman, C. P. Rinsland, A. Goldma, S. T. Massie, D. P. Edwards, J.-Y. Mandin, J. Schroeder, A. McCann, R. R. Gamache, R. B. Wattsin,

K. Yoshino, K. V. Chance, K. W. Juck, L. R. Brown, V. Nemtchechin and P. Varanasi, *J. Quant. Spectrosc. Radiat. Transfer*, 1998, **60**, 665–710.
27 C. R. Webster, R. T. Menzies and E. D. Hinkley, in *Laser Remote Chemical Analysis*, ed. R. M. Measures, Wiley & Sons, New York, 1987, pp. 163–172.
28 H. I. Schiff, G. I. Mackay and J. Bechara, in *Air Monitoring by Spectroscopic Techniques*, ed. M. W. Sigrist, Wiley & Sons, New York, 1994, pp. 219–334.
29 P. Werle, *Spectrochim. Acta A*, 1998, **54**, 197–236.
30 J. A. Silver, *Appl. Opt.*, 1992, **31**, 707–716.
31 M. Gabrysch, C. Corsi, F. S. Pavone and M. Inguscio, *Appl. Phys. B*, 1997, **65**, 75–79.
32 R. Engelbrecht, PhD Thesis, University Erlangen-Nuremberg, Germany, 2001.
33 F. Marin, A. Bramati, V. Jost and E. Giacobo, *Opt. Commun.*, 1997, **140**, 146–157.
34 J. Ye, L. S. Ma and J. L. Hall, *J. Opt. Soc. Am. B*, 1998, **15**, 6–15.